Probing Ion-Receptor Interactions in Halide Complexes of Octamethyl Calix[4]Pyrrole

Lane M. Terry,[a] Madison M. Foreman,[a] Anne P. Rasmussen,[a,b] Anne B. McCoy,[c,#] and J. Mathias Weber[a,]*

[a] JILA and Department of Chemistry, University of Colorado, 440 UCB, Boulder, CO 80309-0440, USA.

[b] Department of Physics and Astronomy, Aarhus University, 8000 Aarhus, Denmark

[c] Department of Chemistry, University of Washington, Seattle, WA 98195, USA

ABSTRACT. The interplay of solvation and ion binding in anion host-guest complexes in solution governs the binding efficiency and selectivity of ion receptors. To gain molecular-level insight into the intrinsic binding properties of octamethyl calix[4]pyrrole (omC4P) host molecules with halide guest ions, we performed cryogenic ion vibrational spectroscopy (CIVS) of omC4P in complexes with fluoride, chloride, and bromide ions. We interpret the spectra using density functional theory, describing the infrared spectra of these complexes with both harmonic and anharmonic VPT2 calculations. The NH stretching modes of the pyrrole moieties serve as sensitive probes of the ion binding properties, as their frequencies encode the ion-receptor interactions. While scaled harmonic spectra reproduce the experimental NH stretching modes of the chloride and bromide complexes in broad strokes, the high proton affinity of fluoride introduces strong anharmonic effects. As a result, the spectrum of F^-·omC4P is not even qualitatively captured by harmonic calculations, but it is recovered very well by VPT2 calculations. In addition, the VPT2 calculations recover the intricate coupling of the NH stretching modes with overtones and combination bands of CH stretching and NH bending modes and with low-frequency vibrations of the omC4P macrocycle, which are apparent for all halide ion complexes investigated here. A comparison of the CIVS spectra with infrared spectra of solutions of the same ion-receptor complexes shows how ion solvation changes the ion-receptor interactions for the different halide ions.

TOC Figure

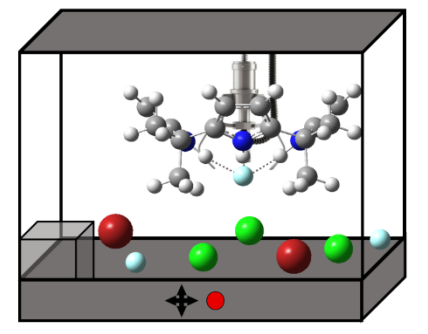

Introduction

Synthetic molecular ion receptors have long been a focus of attention in supramolecular chemistry.[1-7] Applications of molecular recognition of ions address the need to measure and control the concentrations of ionic species in numerous chemical contexts, ranging from ionophore antibiotics[8-9] to sensing,[10-13] materials science,[14] and separation science.[10] Ion recognition also has impact on important issues regarding food and water sources, such as the safety of public water supplies,[15-18] or pollution with nitrate and phosphate from agriculture.[19]

For anions in particular, a complete, predictive understanding of noncovalent interactions in ion receptors in solution has not been achieved to date, despite decades-long work on molecular recognition complexes,[1, 3, 6, 20-25] and there is still a need for a detailed, fundamental understanding of ion receptors and binding competitiveness in solution in order to advance the rational design of synthetic hosts for ionic guests.[6, 21, 23] Experimental work in solutions (in particular NMR spectroscopy) has been instrumental for obtaining structural data of the host-guest complexes themselves. However, effects of solvation are much more difficult to account for,[21, 23] particularly the interaction of the immediate solvation environment (i.e., the first solvation shell) with both receptor and ion and its effect on the structure of and intermolecular forces in host-guest complexes.

In principle, infrared (IR) spectroscopy is very well suited to inform on the intermolecular forces involved in the interaction of ions, both with receptors and with their chemical environment, but the spectroscopic responses encoding the relevant interactions in solutions are often obscured by other absorption features. This is particularly true for the noncovalent interactions in aqueous

environments, both between ion and receptor, and between either partner with solvent molecules. However, these interactions are crucial for molecular recognition, as they govern the competitiveness for ion binding by a receptor compared to ion solvation. Another difficulty associated with the analysis of solution data is the possibility of speciation. For example, polyprotic receptors or ionic guests can exist in different protonation or deprotonation states, host-guest complexes can exist with or without counter ions in close proximity, and they can be surrounded by different (and fluctuating!) numbers of solvent molecules. This lack of control over the chemical environment of the host-guest complex is hindering the precise characterization of the complex and its interaction with the solvation shell.

An attractive approach to the detailed characterization of the relevant interactions is to use mass spectrometric preparation of the relevant ionic complexes by ESI in tandem with laser spectroscopy. This strategy circumvents many of the complications present in solutions, as mass selection reduces ambiguities from speciation and completely removes any masking background signals from the bulk. In particular, spectroscopy of mass selected ions allows the characterization of structures and intermolecular forces in the absence of solvent to contrast with solution phase data, offering direct, experimental access to the characterization of solvent effects.

In this work, we present cryogenic ion vibrational spectroscopy and density functional theory calculations combined with anharmonic calculations of the spectra. These approaches are used to probe the interaction of halide guest ions with octamethyl calix[4]pyrrole hosts, shown in Figure 1. Calix[4]pyrroles (C4Ps) are macrocycles consisting of four pyrrole moieties linked by fully substituted sp^3 *meso*-carbon atoms. In principle, C4Ps can have multiple conformations, characterized by the relative orientations of their pyrrole groups. In nonpolar solvents, the direction

of their NH groups usually is non-uniform, but in polar solvents, they predominantly have a conical conformation[26] with roughly C_{4v} symmetry and the NH groups forming a polar binding site. Octamethyl calix[4]pyrrole (omC4P) is a prototypical ion receptor in this class of molecules, which has been studied in solution by several groups (see, e.g., Refs. 26-29). The axial methyl groups around the cone formed by the four NH groups form a shallow binding pocket. Earlier solution-phase studies showed that omC4P binds strongly to F^- and Cl^-, less so to Br^-, and not significantly to I^-.[27-28] We probe the interaction of halide ions with omC4P by analyzing the vibrational spectra of cryogenically prepared X^-·omC4P complexes *in vacuo*. In this approach, the NH stretching modes of the complexes serve as sensitive probes of the anion-omC4P interaction, and we compare these spectra with analogous spectra obtained from room temperature solutions. We interpret the experimental spectra with calculated IR spectra obtained by density functional theory (DFT), both in the harmonic approximation and through vibrational perturbation theory (VPT2).

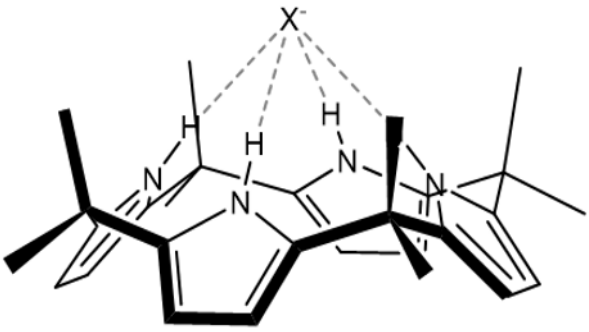

Figure 1. Generic structure of halide-omC4P complexes.

Experimental Methods

Our cryogenic ion vibrational spectroscopy setup has been described in detail in earlier work,[30] and only a brief overview will be given here. Solutions for electrospray ionization contained equimolar amounts of halide salts and omC4P (ChemScene) in mixtures of acetonitrile (ACN, Thermo Fisher Scientific) and water, using 0.1 mM of tetrabutylammonium fluoride (Thermo Fisher Scientific) and 1:1 ACN:H_2O, 0.5 mM sodium chloride (Sigma-Aldrich), and 0.01 mM potassium bromide (Sigma-Aldrich) for X = F, Cl, and Br, respectively. All chemicals were used as purchased.

Halide-omC4P ions, $X^-\cdot$omC4P, were generated by electrospray ionization. Ions from the spray entered a heated desolvation capillary (80 °C), followed by a skimmer. They were then guided through a series of radiofrequency octopole ion guides, a quadrupole bender, and electrostatic ion lenses into a 3D Paul trap, which was kept at ca. 30 K by a closed-cycle He cryostat. The ions in the trap were subjected to buffer gas cooling (10% D_2 in He). The presence of residual N_2 gas from the source inlet resulted in the formation of adduct ions of the form $X^-\cdot$omC4P$\cdot N_2$ in the trap (N_2 messenger tagging). The trap contents were injected into the acceleration region of a Wiley-McLaren time-of-flight mass spectrometer (TOF-MS) with a repetition rate of 20 Hz. In the first space focus of the TOF-MS, the ions with N_2 adducts were mass-selected by a pulsed interleaving comb mass gate and irradiated with the output from a tunable IR OPO/OPA system (LaserVision). The binding energy of the N_2 molecules is sufficiently small that absorption of a single IR photon in the mid-IR results in enough heating of the

$X^-\cdot$omC4P$\cdot N_2$ target ions to induce the loss of the N_2 moiety by unimolecular decay, following the reaction

$$X^-\cdot\text{omC4P}\cdot N_2 + \hbar\omega_{IR} \rightarrow X^-\cdot\text{omC4P} + N_2.$$

The fragment ions, $X^-\cdot$omC4P, were separated from the target ions using a reflectron as a secondary mass spectrometer and detected on a dual microchannel plate detector. The fragment ion intensity was monitored as a function of the photon energy and normalized to the photon fluence to obtain the relative photofragmentation yield. The light source was fired during every other experimental cycle to allow background subtraction. Several of the resulting photodissociation spectra were averaged and retaken on different days to ensure reproducibility and improve the signal-to-noise ratio.

Fourier Transform IR (FTIR) spectra of solutions of the halide-omC4P complexes were acquired with a Thermo Scientific Nicolet iS5 FTIR spectrometer using a Starna Cell Infrasil cylindrical cell with 0.2 mm path length. Solutions were prepared by dissolving equimolar amounts of omC4P and tetrabutylammonium halide salts (TCI America) in CD_3CN (Thermo Scientific Chemicals) at 10 mM concentration.

Computational Methods

The structures and spectra of $X^-\cdot$omC4P complexes (X = F, Cl and Br) were calculated using DFT,[31] with the B3LYP functional.[32-33] In this work, we used the cc-pVDZ basis sets for all C

atoms, and aug-cc-pVDZ basis sets for all other atoms.[34] The difference in the basis sets reflects the greater importance of diffuse functions for the halide ion and the atoms it is most closely interacting with (e.g. the nitrogen and hydrogen atoms) and the computational expense of frequency calculations using the full aug-cc-pVDZ basis. All calculations were performed using Gaussian 16.[35] To better compare to the patterns of the experimental spectra, the harmonic frequencies used to generate the IR spectra calculated for these structures were scaled by 0.9529 to match the NH stretching frequency belonging to the *e* mode in the experimental spectrum of Cl^{-}·omC4P. Binding energies of the halide ions to omC4P were calculated including the counterpoise correction.[36-37]

To aid in the assignment of the spectra, we employed two additional types of calculations, both of which are based on the vibrational perturbation theory (VPT2) calculations that are implemented in Gaussian 16.[35] Second order vibrational perturbation theory requires a quartic expansion of the potential and a cubic expansion of the dipole surface. As implemented in the Gaussian program, these expansions are obtained by displacing each of the normal mode coordinates from its equilibrium value in both the positive and negative direction and evaluating the Hessian and dipole derivatives at each of these displaced geometries. This information allows for the evaluation of the third and fourth derivatives of the potential as well as second and third derivatives of the dipole surface using finite difference schemes.[38-40]

The complexes explored in the present study contain 69 atoms and have 201 normal modes, and the above approach is impractical even at the relatively inexpensive level of electronic structure theory that we are using. On the other hand, in the absence of near degeneracies, the most

important cubic and quartic terms in the expansion of the potential that contribute to the evaluation of the transition frequency (e.g. $E - E_0$) for a state with one or more quanta of excitation in mode n are those that involve differentiation of the potential with respect to q_n. While other terms contribute to the absolute energies, most do not affect the energy differences. The exception are terms of the form $\partial^3 V/\partial q_i q_j q_j$, where $i, j \neq n$. In general, these terms can be expected to introduce a small correction to the energy. Performing the perturbation theory in a reduced dimensional space greatly reduces the expense of the potential evaluation as, if we are only interested in excitation in a subset of the vibrations, we can use a restricted expansion of the potential that only includes terms that involve derivatives with respect to these normal mode coordinates. While the use of this restricted expansion will also lead to approximations in the calculated intensities for $\Delta v = 1$ transitions, the leading contribution to these intensities comes from the linear dipole/harmonic oscillator approximation. We have validated the accuracy of this treatment through reduced-dimensional perturbation theory calculations of the F^--bound NH stretching vibrations in $F^-\cdots HNH_2$ and $F^-\cdots HN(CH_3)_2$ (see Supporting Information). These calculations were used to explore the anharmonicity and Fermi-resonance couplings among the four NH stretching vibrations and the four NH wags as well as the eight highest frequency CH stretching vibrations.

In addition to the reduced dimensional VPT2 calculations, we used the cubic force constants obtained from the VPT2 calculations to construct a reduced-dimensional Hamiltonian matrix that consists of the four NH stretches, any states with two quanta in the NH wags that are strongly coupled to the NH stretching states, and the low-frequency vibrations that are coupled to the NH

stretches through cubic terms in the potential. These vibrational modes were identified by considering the low-frequency vibrations with frequencies below 500 cm^{-1} and with cubic coupling terms involving one low-frequency vibrations and two of the NH stretching vibrations that exceed 20 cm^{-1}. For the F^-·omC4P, the calculation considered eight states with two quanta in the NH wags and ten low-frequency vibrations, while for the Cl^-·omC4P and Br^-·omC4P complexes, only the NH stretching and eight low-frequency vibrations were included in the calculations.

The above approach is based on an earlier study by one of us on host-guest complexes of a hydronium ion in the 18-crown-6 ether,[41] which itself was based on a recognition that low-frequency motions of such complexes can tune the very anharmonic XH stretching frequencies.[42] In developing the present model, we considered all states with one quantum of excitation in the high-frequency NH stretching vibration and up to three quanta of excitation distributed among the low-frequency vibrations. The calculation was repeated with a larger basis, and we found that increasing the total excitation in the low-frequency vibrations had little effect on the calculated spectrum. The intensities are obtained by using the transition moments for the deperturbed 1-0 transitions for the NH-stretching vibrations and assuming that transitions to states with excitation in both the NH stretch and low frequency vibrations carry no intrinsic intensity. A list of the frequencies and cubic coupling terms that were used to set up the Hamiltonian matrix in this reduced-dimensional space along with a list of the calculated eigenstates and their intensities are provided in the Supporting Information.

Results and Discussion

Figure 2 shows the IR photodissociation spectra of N_2-tagged Cl^-·omC4P and Br^-·omC4P together with their calculated IR spectra. The halide-omC4P complexes have C_{4v} symmetry, and consequently each vibrational mode of the omC4P macrocycle is a linear combination of the local modes of the symmetry-linked constituents. We note that not all linear combinations of local oscillators are IR active due to the symmetry of the complex. To assist in the assignment, each calculated spectrum is shown as an inverted plot below the corresponding experimental spectrum. The calculated spectra are evaluated using a combination of the three calculations described above. Specifically, the frequencies and intensities of transitions involving the pyrrole CH stretching and NH wagging vibrations are obtained from a VPT2 calculation that only considers these twelve modes. The NH stretching and low-frequency vibrations are obtained from an analysis of the cubic terms obtained from a VPT2 calculation that only considers these four high frequency vibrations. Finally, the remaining CH stretching vibrations are treated at the harmonic level, with the frequencies scaled by 0.9529. To differentiate these contributions to the spectra, they are plotted in blue, red, and black in the displayed stick spectra, respectively. The peak positions of the features discussed below are summarized in Table 1, together with the calculated values.

We will address the spectrum of Cl^-·omC4P first. The group of features between 2800 cm^{-1} and 3050 cm^{-1} (labeled "CH_3" in Figure 2) is due to the CH stretching modes of the eight methyl groups. There are likely to be Fermi resonances with the overtones and combination bands of the HCH bending modes in this region,[43] which explains why the features in this region are more complex and congested than predicted by the scaled harmonic calculations shown in Figure 2 and

listed in Table 1. Overtones and combination bands of HCH bending modes often introduce congestion and complicate assignments in the CH_3 stretching region. Since these modes carry little information on the interaction between the ion and the receptor, we will not attempt to assign all features in detail. However, we can tentatively attribute the lower frequency peaks at 2874 cm^{-1} and 2899 cm^{-1} to linear combinations of the local symmetric stretching modes of the CH_3 groups, while the peaks at 2953 cm^{-1} and 2970 cm^{-1} are the signatures of similar linear combinations of asymmetric stretching modes of these groups.

The partially resolved doublet at 3113 cm^{-1} and 3118 cm^{-1} (labeled "CH_{Py}" in Figure 2) is consistent with the calculated frequencies of the CH stretching modes on the pyrrole rings, with the lower frequency component coming from linear combinations of the local antisymmetric modes of the local oscillators, while the higher frequency component is due to linear combinations of the symmetric modes. This assignment is supported by VPT2 calculations that include the eight CH_{Py} stretching vibrations as well as the overtone and combination bands involving the NH wagging vibrations (blue stick spectrum). As seen in the upper panel of Figure 2, the NH wagging overtones lie between the CH_{Py} and NH stretching vibrations, and these transitions pick up notable intensity from Fermi resonances. While these calculations underestimate the intensities of these transitions relative to the NH stretching vibrations, the relative intensities of the two broad peaks around 3170 cm^{-1} (labeled $2NH_B$) and the CH_{Py} features are consistent with the reported spectrum.

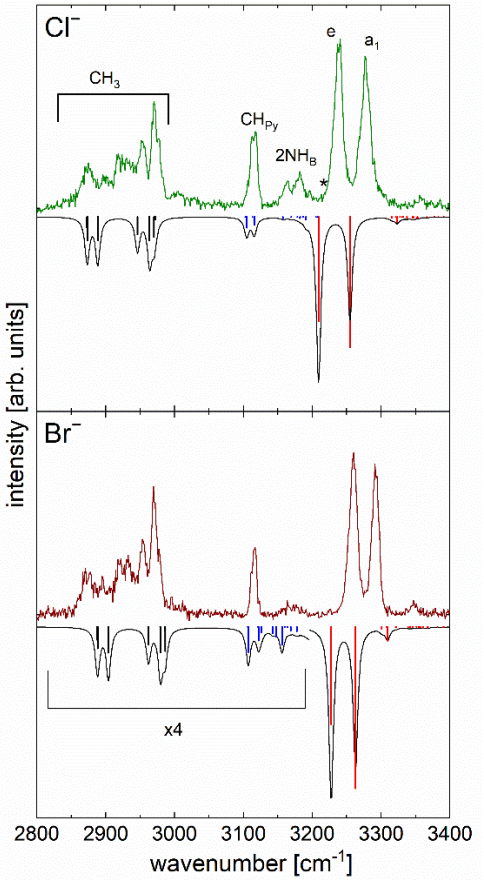

Figure 2. Experimental IR photodissociation spectra (upright) of Cl^-·omC4P·N_2 (top) and Br^-·omC4P·N_2 (bottom) and calculated IR spectra (sticks and full line, inverted) for Cl^-·omC4P and Br^-·omC4P. All calculated features except the CH_3 stretching modes are from anharmonic calculations (see Computational Methods section). The halide ion is indicated in each panel and the experimental traces are color coded for each ion. Individual transitions are represented by vertical bars and distinguished through their method of calculation (black: harmonic, CH_3 stretching modes; blue: VPT2, pyrrole CH stretching fundamental transitions and bending overtones and combination bands, NH wagging overtones and combination bands, includes coupling with NH stretching; red: VPT2, NH stretching fundamental transitions and combination bands with low-frequency vibrational modes). See text for the description of peak labels. For X = Br, the region indicated by the bracket (below 3195 cm^{-1}) in the calculated spectrum was multiplied by a factor of 4 to better show the individual transitions.

Table 1. Selected experimental, scaled harmonic, and anharmonic vibrational frequencies of halide-omC4P complexes in cm^{-1}.

Halide	Experimental	Harmonic	Anharmonic	Characterization
F^-	2870, 2900[a]	2871 – 2887[b]		CH_3 symmetric stretching
	2955, 2974[a]	2942 – 2973[b]		CH_3 asymmetric stretching
	3117	3080, 3096[c]		CH_{Py} antisymmetric stretching
	ca. 2974[c]	3066 (3106)[e]	2987	Degenerate NH stretching (*e*)
	ca. 3100[c]	3194 (3205)[e]	3125	Symmetric NH stretching (a_1)
Cl^-	2874, 2899[a]	2873 – 2889[b]		CH_3 symmetric stretching
	2953, 2970[a]	2945 – 2972[b]		CH_3 asymmetric stretching
	3113	3083		CH_{Py} antisymmetric stretching
	3118	3098		CH_{Py} symmetric stretching
	3239 (3260)[d]	3239 (3289)[e]	3212	Degenerate NH stretching (*e*)
	3277 (3295)[d]	3283 (3313)[e]	3256	Symmetric NH stretching (a_1)
Br^-	2873, 2895[a]	2873 – 2889[b]		CH_3 symmetric stretching
	2954, 2970[a]	2946 – 2971[b]		CH_3 asymmetric stretching
	3117	3083, 3099[c]		CH_{Py} antisymmetric stretching
	3260 (3303)[c,d]	3272 (3319)[e]	3229	Degenerate NH stretching (*e*)
	3292 (3303)[c,d]	3304 (3336)[e]	3263	Symmetric NH stretching (a_1)

[a] Peak centroids.

[b] Range of calculated features with this character.

[c] Experimental features unresolved.

[d] Values in parentheses are from FTIR spectra in CD_3CN solutions.

[e] Values in parentheses are from calculations in a polarizable continuum with the dielectric constant of acetonitrile.

The feature at 3239 cm^{-1} is the signature of two degenerate linear combinations of the local NH stretching oscillators, giving rise to two *e* modes, while the peak at 3277 cm^{-1} is the radially symmetric linear combination, resulting in a mode with a_1 symmetry. These two NH stretching features encode the interaction between the omC4P binding site and the halide ion. The fourth linear combination of the local NH stretching oscillators results in a b_1 mode, whose fundamental transition (scaled harmonic value 3230 cm^{-1}, anharmonic 3204 cm^{-1}) is symmetry forbidden, and therefore missing from the spectrum.

On the basis of these calculations, we can assign the features labeled $2NH_B$ around 3170 cm^{-1} to overtones and combination bands of pyrrole ring deformation/NH wagging modes, which borrow intensity from the intense NH stretching modes. Finally, a weak peak at 3358 cm^{-1} (labeled with an asterisk) is a combination band of the degenerate NH stretching modes with low-frequency modes, particularly a degenerate mode characterized by pyrrole twisting and a side-to-side motion of the Cl^- ion (see Supporting Information, unscaled harmonic frequency 113 cm^{-1}), perpendicular to the symmetry axis of the molecule.

As expected, the CH stretching features do not significantly change their positions upon exchanging Cl^- with Br^- (see Table 1). However, the NH stretching signatures move considerably to the blue, by 21 cm^{-1} and 14 cm^{-1} for the NH(*e*) and NH(a_1) modes, respectively. The blue shift is qualitatively consistent with the change in proton affinity of the halide (1395 kJ/mol for Cl^- [44] and 1354 kJ/mol for Br^- [45]), as well as the calculated binding energy to omC4P (2.37 eV for Cl^-, 2.04 eV for Br^-). The weaker interaction of the NH groups with Br^- leads to a shift of the NH stretching modes towards their value for free, neutral omC4P (highest calculated, scaled harmonic

value 3448 cm^{-1}, see Supporting Information). Both the harmonic and anharmonic calculations qualitatively capture the frequency shift between the Cl^- and Br^- complexes.

Along the same lines of thought, one would expect the NH stretching modes to shift to lower frequencies for ions with a greater proton affinity. Figure 3 shows the IR spectrum of N_2 tagged F^-·omC4P. At first glance, the NH stretching bands seem to be absent from the spectrum, and they are not recovered at all by calculations based on the harmonic approximation (Figure 3). In addition, there are many additional bands at frequencies above the range of the CH_3 signatures, more than observed for the bromide and chloride complexes. The CH_3 signatures themselves are in line with those found for the other X^-·omC4P complexes, and although the CH_{Py} feature shows some broadening on its low frequency side, its peak and high frequency side are compatible with CH_{Py} features largely unaffected by the change in the chemical identity of the ion.

We note that in light of the large proton affinity of F^-, one might hypothesize that the complex does not adopt C_{4v} symmetry at all, and instead have a minimum structure with the F^- ion displaced towards one of the NH groups. Such a structural change might well lead to a completely different pattern of the NH stretching features. However, a structural search explicitly testing for such motifs did not reveal any indication for a deviation from C_{4v} symmetry.

Anharmonic (VPT2) calculations offer an explanation for both the apparently missing NH stretching signatures and for the additional features above ca. 3030 cm^{-1}. The VPT2 calculations predict the NH(e) and NH(a_1) transitions at 2987 cm^{-1} and 3125 cm^{-1}, respectively, highlighting the lowered frequencies and larger anharmonicities of these modes compared to the Cl^- and Br^- complexes, which we attribute to the very large proton affinity of F^- (1555 kJ/mol for F^- [46]), which also results in a large calculated binding energy to omC4P (3.89 eV). While the intensity of the

NH(*e*) feature is overestimated, transitions based on strongly anharmonic OH or NH oscillators are typically not only significantly red-shifted, but also very broad,[41, 47-52] making it possible that the mode will be broadened sufficiently to be all but unobservable in the congested CH_3 stretching region. The stronger coupling is evidenced by the more extended series of combination transitions involving the NH stretching vibration and low frequency motions, indicated by arrows in Figure 3. We note that exploratory measurements in the frequency range below 2800 cm^{-1} did not reveal any features that would indicate an even greater red shift of the NH(*e*) mode. The NH(a_1) transition is predicted by the VPT2 calculations to be found in the same region as the CH_{Py} transitions, most likely contributing to the broad shoulder around 3100 cm^{-1}.

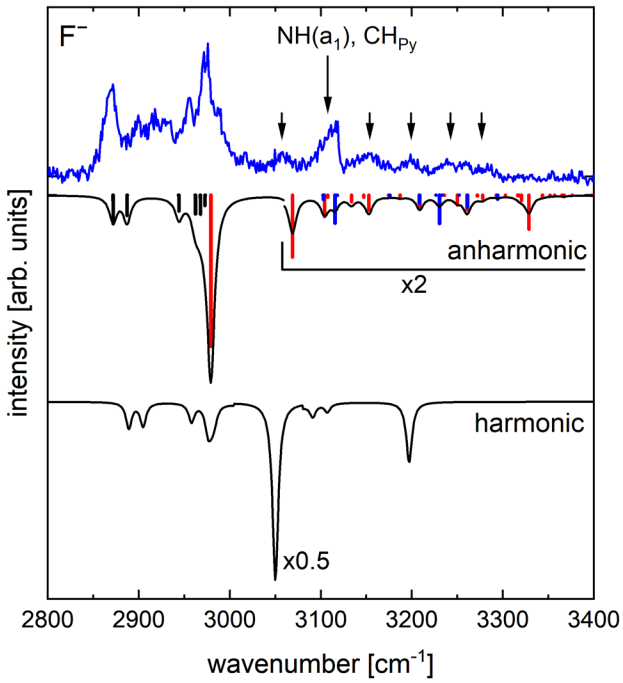

Figure 3. IR photodissociation spectrum of F^-·omC4P·N_2 (upright, top), in comparison with the calculated IR spectrum from a VPT2 calculation (inverted, sticks and full line, second trace from top, color scheme as in Figure 2), and from a scaled harmonic calculation (inverted, bottom). The intensity of the strongest transition in the harmonic spectrum was multiplied by 0.5 for better comparison between the spectra. Similarly, the region indicated by the bracket (above 3080 cm^{-1}) in the anharmonic spectrum was multiplied by a factor of 2 to better show the sequence bands of low frequency vibrations coupling to the NH(*e*) mode, which are also indicated by the short arrows.

The pronounced anharmonic nature of the NH stretching potential in F^-·omC4P also introduces strong coupling with low frequency vibrational modes that tune the NH···F^- angle, and therefore the NH···F^- interaction (see Supporting Information). This coupling can then give rise to the observation of sequence bands of such low frequency modes,[41-42, 47-52] building on the transition of the NH stretching mode coupling to them. The broad, new features above 3050 cm^{-1} are

consistent with such sequence bands, gaining significant intensity through anharmonic coupling to the NH(*e*) mode.

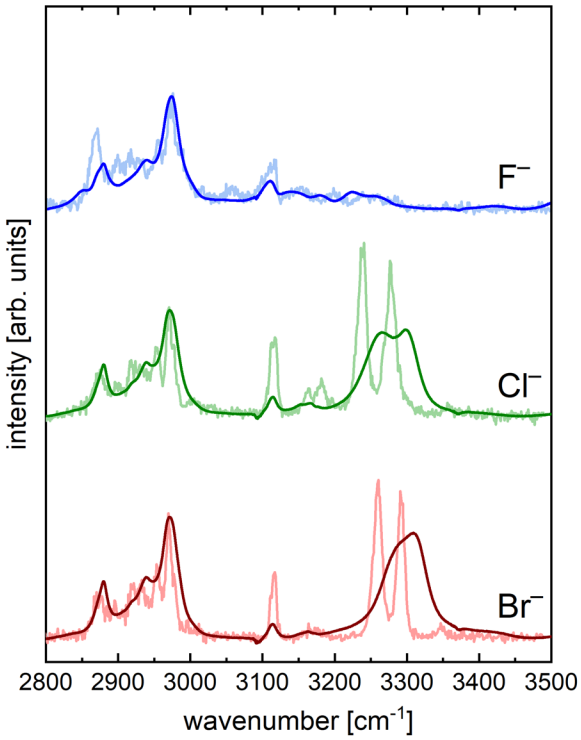

Figure 4. Comparison of experimental IR photodissociation spectra of halide-omC4P complexes (faded lines) with FTIR spectra of 10 mM solutions of the same complexes in CD_3CN (full lines). The identity of each halide is given above each trace.

One of the main challenges in the design of anion receptors is to accurately account for the effects of solvation on the ion binding. Figure 4 shows a comparison of the IR photodissociation spectra of the halide-omC4P complexes under study with the FTIR spectra of solutions of the same complexes in CD_3CN. The frequencies of the CH stretching features are rather insensitive to the chemical environment (vacuum vs. solution). The NH stretching features for complexes with Cl^-

and Br^- shift towards higher frequencies (on average 20 cm^{-1} for Cl^- and 27 cm^{-1} for Br^-). This behavior is not unexpected, as the interaction between the ion and the solvent will serve to weaken the interaction between the ion and the binding site of the omC4P receptor. The competition between ion binding and ion solvation is of course at the heart of the change of the equilibrium binding constant between the different halides, which increases by a factor of 35 from Br^- to Cl^-, and by a factor of 49 from Cl^- to F^- for solutions in CD_2Cl_2.[27]

In contrast to the complexes with Br^- and Cl^-, there is very little overall change in the spectral envelope for F^-·omC4P. In particular, there is no indication that the NH stretching modes shift to higher frequencies at all. A look at the geometries of the complexes (Figure 5) holds clues to explain this behavior. As the NH···X^- distance diminishes from Br^- to F^-, the exposure of the halide ion to the chemical environment diminishes as well, owing to the changes in the proton affinities along the halide series. While both Br^- and Cl^- ions protrude significantly beyond the plane of the axial methyl groups of the complex, F^- is sufficiently deep in the binding pocket to have very little direct exposure to the solvent, and therefore does not exhibit any significant solvent-induced change in the NH stretching signatures. Scaled harmonic calculations embedding Cl^-·omC4P and Br^-·omC4P complexes in a dielectric medium (simulated by a polarizable continuum model[53]) with the dielectric constant of acetonitrile (35.688 as implemented in Gaussian 16) qualitatively recover the blue shift of the NH stretching modes, but overestimate the amount (see Table 1). Analogous calculations on F^-·omC4P predict a similar blue shift as for the Cl^- and Br^- complexes, which is contrary to the experimental observations. This is not surprising, since the harmonic calculations underestimate the red shift of the NH stretching modes in F^-·omC4P and would therefore likely overestimate the influence of the solvent on their frequencies. In line

with the predicted change in frequencies, the presence of a dielectric medium results in increases in the NH···X^- distances (by 3 – 5%, see Figure 5). We note that based on work by Flood and coworkers,[23] the calculated binding energies and NH···X^- distances put all halide-omC4P complexes into a regime where electrostatic effects dominate the behavior of the complexes, while non-electrostatic interactions (induction and dispersion) do not play a significant role.

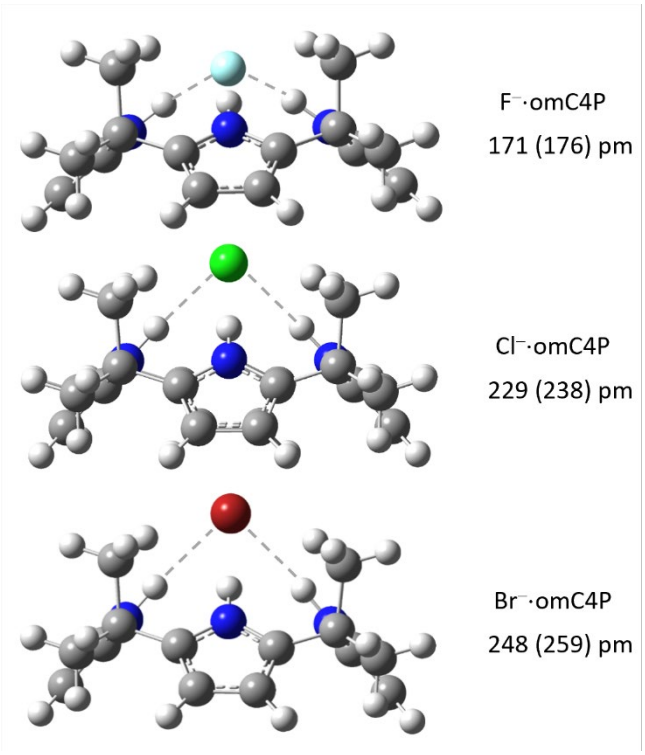

Figure 5. Calculated geometries of gas-phase halide-omC4P complexes. The halide identity is given for each structure, together with the NH···X^- distance (PCM values in parentheses).

Summary and Conclusions

The IR spectra of halide-omC4P complexes show how the interaction between the halide and the ion binding site is encoded in the frequencies of their NH stretching signatures. As one might expect, the frequencies of these features shift to higher values with decreasing proton affinity and binding energy of the halide, and the calculated NH···X distance increases concomitantly. While scaled harmonic spectra recover the experimental NH stretching features of the chloride and bromide complexes quite well, they fail to predict the spectrum of F^-·omC4P even qualitatively, as the high proton affinity of F^- introduces strong anharmonic effects. Anharmonic calculations capture the overall behavior of the NH stretching modes well. In addition, they show how coupling between the NH stretching modes and low frequency motions give rise to additional features in the spectra of all halide-omC4P complexes.

The NH stretching modes observed in vacuo are also observed in solutions of these complexes in CD_3CN. The solvent environment introduces blue shifts in the NH stretching modes for Cl^-·omC4P and Br^-·omC4P compared to their positions in vacuo, but not for F^-·omC4P. We trace the difference in solvent response to the different exposure of the bound ion to the chemical environment. Based on the calculated binding energies and NH···X^- distances, we assume that the interaction between the receptor and the ion is dominated by electrostatics.

ASSOCIATED CONTENT

Supporting Information. The following files are available free of charge:

File 1: Reduced-dimensional perturbation theory calculations of the F^--bound NH stretching vibrations; frequencies, cubic coupling terms, the calculated eigenstates and their intensities; calculated lowest energy structure and NH stretching frequencies for neutral omC4P; atomic coordinates of X^-·omC4P (X = F, Cl, Br);

File 2: Animations of low frequency molecular vibrations coupling to the NH stretching modes for Cl^-·omC4P and F^-·omC4P.

File 3: Excel file containing the parameters used in the calculation that couples the NH stretching vibrations with the low frequency vibrations.

AUTHOR INFORMATION

Corresponding Author

*J. Mathias Weber: weberjm@jila.colorado.edu

#Anne B. McCoy: abmccoy@uw.edu

Notes

The authors declare no competing financial interests.

ACKNOWLEDGMENT

J.M.W. gratefully acknowledges support by the National Science Foundation under award no. CHE-2154271. A.B.M is grateful for support from the National Science Foundation through award no. CHE-2154126. This work utilized resources from the University of Colorado Boulder Research Computing Group, which is supported by the National Science Foundation (awards ACI-1532235 and ACI-1532236), the University of Colorado Boulder, and Colorado State University. We thank Prof. Pablo Ballester and Dr. Gemma Aragay (Institut Català d'Investigació Química, Tarragona, Spain) for helpful discussions on the chemistry of calix[4]pyrroles.

REFERENCES

(1) Hua, Y.; Flood, A. H. Click Chemistry Generates Privileged CH Hydrogen-Bonding Triazoles: The Latest Addition to Anion Supramolecular Chemistry. *Chem. Soc. Rev.* **2010,** *39*, 1262-1271.

(2) Kubik, S. Anion Recognition in Aqueous Media by Cyclopeptides and Other Synthetic Receptors. *Acc. Chem. Res.* **2017,** *50*, 2870-2878.

(3) Cremer, P. S.; Flood, A. H.; Gibb, B. C.; Mobley, D. L. Collaborative Routes to Clarifying the Murky Waters of Aqueous Supramolecular Chemistry. *Nature Chem.* **2018,** *10*, 8-16.

(4) Kubik, S. *Supramolecular Chemistry in Water*. John Wiley & Sons, Inc.: Newark, 2019.

(5) Zhao, W.; Flood, A. H.; White, N. G. Recognition and Applications of Anion–Anion Dimers Based on Anti-Electrostatic Hydrogen Bonds (AEHBs). *Chem. Soc. Rev.* **2020,** *49*, 7893-7906.

(6) Escobar, L.; Ballester, P. Molecular Recognition in Water Using Macrocyclic Synthetic Receptors. *Chem. Rev.* **2021,** *121*, 2445-2514.

(7) Dong, J.; Davis, A. P. Molecular Recognition Mediated by Hydrogen Bonding in Aqueous Media. *Angew. Chem. Int. Ed.* **2021,** *60*, 8035-8048.

(8) Duax, W. L.; Griffin, J. F.; Langs, D. A.; Smith, G. D.; Grochulski, P.; Pletnev, V.; Ivanov, V. Molecular Structure and Mechanisms of Action of Cyclic and Linear Ion Transport Antibiotics. *Biopolymers* **1996,** *40*, 141-155.

(9) Sato, E.; Hirata, K.; Lisy, J. M.; Ishiuchi, S.; Fujii, M. Rethinking Ion Transport by Ionophores: Experimental and Computational Investigation of Single Water Hydration in Valinomycin-K^+ Complexes. *J. Phys. Chem. Lett.* **2021,** *12*, 1754-1758.

(10) Kolesnichenko, I. V.; Anslyn, E. V. Practical Applications of Supramolecular Chemistry. *Chem. Soc. Rev.* **2017,** *46*, 2385-2390.

(11) Buhlmann, P.; Pretsch, E.; Bakker, E. Carrier-Based Ion-Selective Electrodes and Bulk Optodes. 2. Ionophores for Potentiometric and Optical Sensors. *Chem. Rev.* **1998,** *98*, 1593-1687.

(12) Oesch, U.; Ammann, D.; Simon, W. Ion-Selective Membrane Electrodes for Clinical Use. *Clin. Chem.* **1986,** *32*, 1448-1459.

(13) Kubik, S.; Reyheller, C.; Stüwe, S. Recognition of Anions by Synthetic Receptors in Aqueous Solution. *J. Incl. Phenom. Macrocycl. Chem.* **2005,** *52*, 137-187.

(14) Ariga, K.; Ito, H.; Hill, J. P.; Tsukube, H. Molecular Recognition: From Solution Science to Nano/Materials Technology. *Chem. Soc. Rev.* **2012,** *41*, 5800-5835.

(15) Crompton, T. *Determination of Anions in Natural and Treated Waters*. Spon Press.: 2002.

(16) Greer, M. A.; Goodman, G.; Pleus, R. C.; Greer, S. E. Health Effects Assessment for Environmental Perchlorate Contamination: The Dose Response for Inhibition of Thyroidal Radioiodine Uptake in Humans. *Environ. Health Perspect.* **2002,** *110*, 927-937.

(17) Nordstrom, D. K. Public Health - Worldwide Occurrences of Arsenic in Ground Water. *Science* **2002,** *296*, 2143-2145.

(18) Wang, Y. X.; Li, P.; Guo, Q. H.; Jiang, Z.; Liu, M. L. Environmental Biogeochemistry of High Arsenic Geothermal Fluids. *Applied Geochem.* **2018,** *97*, 81-92.

(19) Smolders, A. J. P.; Lucassen, E. C. H. E. T.; Bobbink, R.; Roelofs, J. G. M.; Lamers, L. P. M. How Nitrate Leaching from Agricultural Lands Provokes Phosphate Eutrophication in Groundwater Fed Wetlands: The Sulphur Bridge. *Biogeochem.* **2010,** *98*, 1-7.

(20) Schmidtchen, F. P. Reflections on the Construction of Anion Receptors - Is There a Sign to Resign from Design? *Coord. Chem. Rev.* **2006,** *250*, 2918-2928.

(21) Liu, Y.; Sengupta, A.; Raghavachari, K.; Flood, A. H. Anion Binding in Solution: Beyond the Electrostatic Regime. *Chem* **2017,** *3*, 411-427.

(22) Molina, P.; Zapata, F.; Caballero, A. Anion Recognition Strategies Based on Combined Noncovalent Interactions. *Chem. Rev.* **2017,** *117*, 9907-9972.

(23) Sengupta, A.; Liu, Y.; Flood, A. H.; Raghavachari, K. Anion-Binding Macrocycles Operate Beyond the Electrostatic Regime: Interaction Distances Matter. *Chem. Eur. J.* **2018,** *24*, 14409-14417.

(24) Eytel, L. M.; Fargher, H. A.; Haley, M. M.; Johnson, D. W. The Road to Aryl Ch···Anion Binding Was Paved with Good Intentions: Fundamental Studies, Host Design, and Historical Perspectives in Ch Hydrogen Bonding. *Chem. Comm.* **2019,** *55*, 5195-5206.

(25) Rizzi, A.; Murkli, S.; McNeill, J. N.; Yao, W.; Sullivan, M.; Gilson, M. K.; Chiu, M. W.; Isaacs, L.; Gibb, B. C.; Mobley, D. L.; Chodera, J. D. Overview of the Sampl6 Host–Guest Binding Affinity Prediction Challenge. *J. Comput. Aided Mol. Des.* **2018,** *32*, 937-963.

(26) Kim, D. S.; Sessler, J. L. Calix[4]Pyrroles: Versatile Molecular Containers with Ion Transport, Recognition, and Molecular Switching Functions. *Chem. Soc. Rev.* **2015,** *44*, 532-546.

(27) Gale, P. A.; Sessler, J. L.; Král, V.; Lynch, V. Calix[4]Pyrroles: Old yet New Anion-Binding Agents. *J. Am. Chem. Soc.* **1996,** *118*, 5140-5141.

(28) Sessler, J. L.; Gross, D. E.; Cho, W. S.; Lynch, V. M.; Schmidtchen, F. P.; Bates, G. W.; Light, M. E.; Gale, P. A. Calix[4]Pyrrole as a Chloride Anion Receptor: Solvent and Countercation Effects. *J. Am. Chem. Soc.* **2006,** *128*, 12281-12288.

(29) Gil-Ramirez, G.; Escudero-Adan, E. C.; Benet-Buchholz, J.; Ballester, P. Quantitative Evaluation of Anion-Π Interactions in Solution. *Angew. Chem. Int. Ed.* **2008,** *47*, 4114-4118.

(30) Xu, S.; Gozem, S.; Krylov, A. I.; Christopher, C. R.; Mathias Weber, J. Ligand Influence on the Electronic Spectra of Monocationic Copper-Bipyridine Complexes. *Phys. Chem. Chem. Phys* **2015,** *17*, 31938-31946.

(31) Parr, R. G.; Yang, W. *Density-Functional Theory of Atoms and Molecules*. Oxford University Press: New York, 1989.

(32) Becke, A. D. Density-Functional Exchange-Energy Approximation with Correct Asymptotic-Behavior. *Phys. Rev. A* **1988,** *38*, 3098-3100.

(33) Lee, C. T.; Yang, W. T.; Parr, R. G. Development of the Colle-Salvetti Correlation-Energy Formula into a Functional of the Electron-Density. *Phys. Rev. B* **1988,** *37*, 785-789.

(34) Dunning, T. H. Gaussian-Basis Sets for Use in Correlated Molecular Calculations .1. The Atoms Boron through Neon and Hydrogen. *J. Chem. Phys.* **1989,** *90*, 1007-1023.

(35) Frisch, M. J.; Trucks, G. W.; Schlegel, H. B.; Scuseria, G. E.; Robb, M. A.; Cheeseman, J. R.; Scalmani, G.; Barone, V.; Petersson, G. A.; Nakatsuji, H.; et al. *Gaussian 16 Rev. C.01*, Wallingford, CT, 2016.

(36) Boys, S. F.; Bernardi, F. The Calculation of Small Molecular Interactions by the Differences of Separate Total Energies. Some Procedures with Reduced Errors. *Mol. Phys.* **1970,** *19*, 553-566.

(37) Simon, S.; Duran, M.; Dannenberg, J. J. How Does Basis Set Superposition Error Change the Potential Surfaces for Hydrogen-Bonded Dimers? *J. Chem. Phys.* **1996,** *105*, 11024-11031.

(38) Yang, Q.; Mendolicchio, M.; Barone, V.; Bloino, J. Accuracy and Reliability in the Simulation of Vibrational Spectra: A Comprehensive Benchmark of Energies and Intensities Issuing from Generalized Vibrational Perturbation Theory to Second Order (GVPT2). *Front. Astron. Space Sci.* **2021,** *8*, 665232.

(39) Schneider, W.; Thiel, W. Anharmonic Force Fields from Analytic Second Derivatives: Method and Application to Methyl Bromide. *Chem. Phys. Lett* .**1989,** *157*, 367-373.

(40) McCoy, A. B.; Boyer, M. A. Exploring Expansions of the Potential and Dipole Surfaces Used for Vibrational Perturbation Theory. *J. Phys. Chem. A* **2022,** *126*, 7242-7249.

(41) Craig, S. M.; Menges, F. S.; Duong, C. H.; Denton, J. K.; Madison, L. R.; McCoy, A. B.; Johnson, M. A. Hidden Role of Intermolecular Proton Transfer in the Anomalously Diffuse Vibrational Spectrum of a Trapped Hydronium Ion. *Proc. Natl. Acad. Sci. U. S. A.* **2017,** *114*, E4706-E4713.

(42) Myshakin, E. M.; Jordan, K. D.; Sibert, E. L.; Johnson, M. A. Large Anharmonic Effects in the Infrared Spectra of the Symmetrical $CH_3NO_2^-\cdot(H_2O)$ and $CH_3CO_2^-\cdot(H_2O)$ Complexes. *J. Chem. Phys.* **2003,** *119*, 10138-10145.

(43) Schneider, H.; Vogelhuber, K. M.; Schinle, F.; Stanton, J. F.; Weber, J. M. Vibrational Spectroscopy of Nitroalkane Chains Using Electron Detachment and Ar Predissociation. *J. Phys. Chem. A* **2008,** *112*, 7498-7506.

(44) Martin, J. D. D.; Hepburn, J. W. Determination of Bond Dissociation Energies by Threshold Ion-Pair Production Spectroscopy: An Improved D(HCl). *J. Chem. Phys.* **1998,** *109*, 8139-8142.

(45) Blondel, C.; Cacciani, P.; Delsart, C.; Trainham, R. High-Resolution Determination of the Electron Affinity of Fluorine and Bromine Using Crossed Ion and Laser Beams. *Phys. Rev. A* **1989,** *40*, 3698-3701.

(46) Christophe, B.; Christian, D.; Fabienne, G. Electron Spectrometry at the μeV Level and the Electron Affinities of Si and F. *J. Phys. B: At. Mol. Opt. Phys.* **2001,** *34*, L281.

(47) Weber, J. M.; Kelley, J. A.; Nielsen, S. B.; Ayotte, P.; Johnson, M. A. Isolating the Spectroscopic Signature of a Hydration Shell with the Use of Clusters: Superoxide Tetrahydrate. *Science* **2000,** *287*, 2461-2463.

(48) Ayotte, P.; Kelley, J. A.; Nielsen, S. B.; Johnson, M. A. Vibrational Spectroscopy of the $F^{-}\cdot H_2O$ Complex Via Argon Predissociation: Photoinduced, Intracluster Proton Transfer? *Chem. Phys. Lett.* **2000,** *316*, 455-459.

(49) Robertson, W. H.; Diken, E. G.; Price, E. A.; Shin, J. W.; Johnson, M. A. Spectroscopic Determination of the OH^- Solvation Shell in the $OH^-\cdot H_2O_n$ Clusters. *Science* **2003,** *299*, 1367-1372.

(50) Blodgett, K. N.; Fischer, J. L.; Zwier, T. S.; Sibert, E. L. The Missing NH Stretch Fundamental in S_1 Methyl Anthranilate: IR-UV Double Resonance Experiments and Local Mode Theory. *Phys. Chem. Chem. Phys.* **2020,** *22*, 14077-14087.

(51) Chen, L. Y.; Ma, Z. F.; Fournier, J. A. Origins of the Diffuse Shared Proton Vibrational Signatures in Proton-Coupled Electron Transfer Model Dyad Complexes. *J. Chem. Phys.* **2022,** *157*, 154308.

(52) Chen, L. Y.; Sibert, E. L.; Fournier, J. A. Unraveling the Vibrational Spectral Signatures of a Dislocated H Atom in Model Proton-Coupled Electron Transfer Dyad Systems. *J. Phys. Chem. A* **2023,** *127*, 3362-3371.

(53) Miertuš, S.; Scrocco, E.; Tomasi, J. Electrostatic Interaction of a Solute with a Continuum. A Direct Utilizaion of Ab Initio Molecular Potentials for the Prevision of Solvent Effects. *Chem. Phys.* **1981,** *55*, 117-129.

TOC Figure